

# Bright Heralded Single-Photon Superradiance in a High-Density Thin Vapor Cell

Heewoo Kim,<sup>1</sup> Bojeong Seo,<sup>2</sup> and Han Seb Moon,<sup>1,2,3,\*</sup>

<sup>1</sup>*Department of Physics, Pusan National University, Busan 46241, South Korea*

<sup>2</sup>*Quantum Science Technology Center, Pusan National University, Busan 46241, South Korea*

<sup>3</sup>*Quantum Sensors Research Center, Pusan National University, Busan 46241, South Korea*

*\*hsmoon@pusan.ac.kr*

Superradiance is a hallmark of cooperative quantum emission, where radiative decay is collectively enhanced by coherence among emitters. Here, extending superradiant effects to photon pair generation from multi-level atoms, two-photon process offers a pathway to novel quantum light sources and a useful case for practical superradiance. We report bright heralded single-photon superradiance via spontaneous four-wave mixing in a 1-mm-long, high-density cesium vapor cell. By reducing the average distance between atoms in the atomic vapor to 0.29 times the idler photon wavelength, we observe a dramatic narrowing of the temporal two-photon wavefunction, from 0.60 ns to 0.17 ns. This compression of temporal two-photon wavefunction evidences the superradiance of heralded photons in the collective two-photon emission dynamics. Furthermore, our heralded single-photon superradiance is accompanied by a coincidence-to-accidental ratio of 200 and the detected photon-pair counting exceeding  $10^6$  pairs/s. These findings establish dense thin atomic vapors as a practical, robust medium for realizing superradiant photon sources, with immediate relevance for quantum optics and the development of efficient photonic quantum technologies.

*Introduction.*—Since the seminal concept of superradiance was introduced by Robert H. Dicke in 1954<sup>1</sup>, it has remained a focal point of research into cooperative emission phenomena for decades. The phenomenon occurs when an ensemble of emitters, such as atoms and solid-state systems including quantum dots and nitrogen-vacancy centers in diamond<sup>2–6</sup>, interact coherently with a common light field, leading to a dramatically accelerated spontaneous decay rate scaling superlinearly with the number of emitters. In the single-excitation regime, superradiant light emerges directionally from an atomic ensemble coupled to a common vacuum mode, facilitated by phase-matched interactions between indistinguishable atoms<sup>7,8</sup>.

As is well known, superradiance arises in a dipole-allowed transition of two-level atoms through quantum fluctuations, leading to the emission of intense radiation whose decay rate scales superlinearly with the number of atoms<sup>1</sup>. However, superradiant emission is not limited to simple two-level transitions. In a three-level cascade-type two-photon transition, the collective effect of photon-pair generation via spontaneous four-wave mixing (SFWM) process can emerge due to two-photon atomic coherence<sup>9,10</sup>. In such an SFWM system, a signal photon is spontaneously generated first, often adiabatically, and acts as a coherent precursor to the subsequent emission of the idler photon. Interestingly, this sequence can be understood as a form of triggered superradiance, where the buildup of macroscopic coherence enables a collectively enhanced decay of the idler photon<sup>9</sup>.

In this work, we report superradiance of bright photon pair from a highly dense and thin Cs vapor cell in the cascade-type  $6S_{1/2}$ – $6P_{3/2}$ – $6D_{5/2}$  transition of  $^{133}\text{Cs}$ . By increasing the atomic density of the 1-mm-scale Cs vapor cell, the average interatomic distance in the ensemble is easily reduced to below the emitted photon wavelength, thereby satisfying the subwavelength condition required for cooperative emission. We refer to this collective two-photon emission as heralded single-photon superradiance (HSSR). We provide the first observation of a sharp temporal feature in the cross-correlation function of HSSR provides compelling evidence of a superradiance, where the collective decay of the heralded idler photon leads to highly directional and synchronized photon-pair emission.

In particular, atomic vapor cells offer a highly accessible and tunable platform for studying cooperative quantum phenomena<sup>11,12</sup> and photonic quantum information technologies<sup>13–21</sup>. Unlike cold atomic systems, thermal vapors enable compact, room-temperature implementations with flexible control over atomic density via temperature. In thermal atomic vapors, the atomic number density is determined by the vapor pressure, and the corresponding interatomic distance is therefore entirely set by this density. Importantly, by adjusting the cell temperature, the density of the atomic ensemble can be tuned over nearly three orders of magnitude, allowing the system to be driven continuously from a dilute, non-cooperative regime where the mean interatomic distance exceeds the optical wavelength to a subwavelength cooperative regime where collective emission effects become prominent.

Furthermore, in our work, the thin geometry of the atomic vapor cell enables higher atomic number densities at a fixed optical depth, allowing the average interatomic spacing to be significantly reduced while maintaining sufficient optical transmission and coherence times. To our knowledge, this constitutes the brightest photon-pair source demonstrated to date in a thermal atomic system. This result shows that HSSR in a high-density warm vapor enables photon-pair brightness far beyond previously reported thermal vapor implementations, establishing warm atomic vapors as a practical platform for superradiance applications and scalable photonic quantum technologies.

*Heralded single-photon superradiance process.*—We describe the heralded single-photon superradiance process, as shown in Fig. 1a. In our cascade-type SFWM scheme under large detuning of pump and coupling fields, the signal photon is generated adiabatically and precedes the emission of idler photon. The pump and coupling lasers interact with the  $6S_{1/2}$ – $6P_{3/2}$  and  $6P_{3/2}$ – $6D_{5/2}$  transitions of  $^{133}\text{Cs}$ , respectively, with detunings  $\delta_p$  and  $\delta_c$  from the corresponding resonances, and a two-photon detuning  $\delta_{\text{two}} = \delta_p + \delta_c$ .

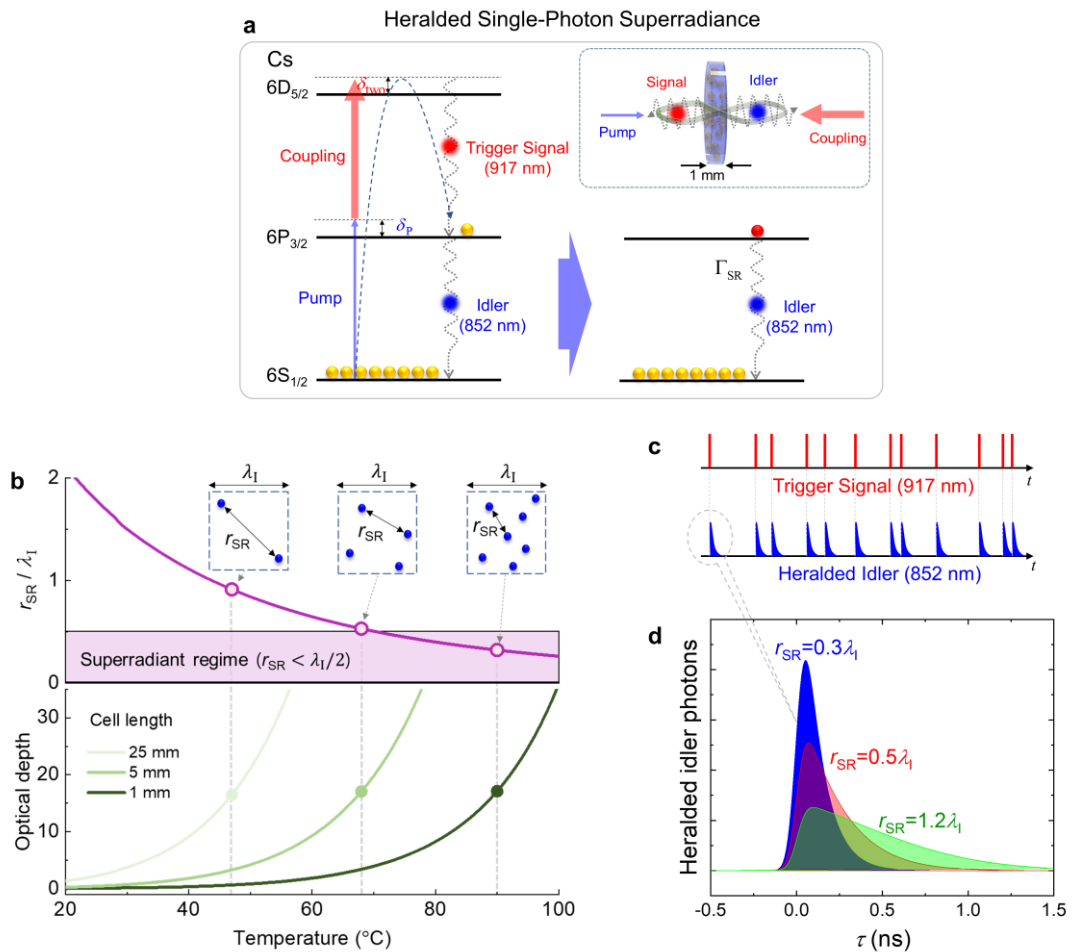


**Fig. 1 Experimental configuration for heralded single-photon superradiance process.** **a**, Heralded superradiance process in three-level cascade-type atomic system. The signal photon plays the role of a trigger photon and the adiabatic excitation prepares the ensemble in a Dicke-like state; the idler photon is spontaneously emitted through the heralded superradiant decay. The inset illustrates the experimental scheme. **b**, Temperature dependence of the average interatomic distance and optical depth for cesium vapor cells of different lengths. For shorter cells, the system reaches the superradiant regime while maintaining moderate optical depth, enabling cooperative emission. **c**, The signal photons are generated under continuous excitation and exhibit thermal photon statistics. When the triggering signal photon defines the start time (gray dashed lines), the heralded idler photons appear in a pulsed temporal mode with a superradiance. **d**, The biphoton wavefunction exhibits pronounced temporal narrowing as the average interatomic distance decreases ( $r_{\text{SR}} = 0.3\lambda_1$ ,  $0.5\lambda_1$ ,  $1.2\lambda_1$ ). Superradiance of the heralded idler photons is observed when  $r_{\text{SR}} < \lambda_1/2$ .

The first step, involving the emission of the signal photon, is initiated by an adiabatic excitation that prepares the ensemble in a Dicke-like state. The single atomic excitation in a collection of atoms in the  $6P_{3/2}$  intermediate state is conditionally prepared as

$$|\Psi\rangle = \frac{1}{\sqrt{N}} \sum_j^N C_j e^{i\delta_j t} e^{i\vec{k}_S \cdot \vec{r}_j} |g_1, \dots, i_j, \dots, g_N\rangle |0\rangle \quad (1)$$

where  $N$  is the number of atoms,  $\vec{k}_S$  is the wave-vector of the signal field,  $\delta_j$  is the detuning of the incident field due to the Doppler shift,  $\vec{r}_j$  is the position of each atom in the ensemble, and  $C_j$  is the probability amplitude of finding atoms in the intermediate state. In this  $N$ -atom entangled state, a single atomic excitation is shared among a large number of atoms.

In the second step, the idler photon is spontaneously emitted via a heralded superradiant decay. The emission of signal photon, adiabatically seeded by a pre-established two-photon coherence, plays the role of a trigger photon that initiates the superradiant decay ( $\Gamma_{SR}$ ) of the idler photon via the HSSR process. In a highly dense atomic medium, where the average interatomic distance is subwavelength, the heralded idler photon undergoes a collective decay characterized by a superradiance strength. Consequently, the probability amplitudes of detecting an idler photon in the phase-matched direction are coherently superposed over the spatial and velocity distributions of atoms, leading to directional enhancement via constructive interference.

The experimental configuration for HSSR in cascade-type atomic system is shown in the inset of Fig. 1a. Counter-propagating pump and coupling lasers interact with a 1-mm-long, thin cesium vapor cell, generating entangled HSSR from a high-density atomic vapor whose density can be tuned by adjusting the cell temperature. Fig. 1b quantitatively shows how the average interatomic distance and optical depth evolve with temperature for vapor cells of different lengths. Increasing the cell temperature increases the atomic number density, thereby reducing the interatomic distance. For sufficiently short cells, the system enters the subwavelength regime while maintaining moderate optical depth, providing favorable conditions for observing heralded superradiant emission. Here, the subwavelength regime ( $r_{SR} < \lambda_I$ ) denotes the onset of cooperative effects, whereas the superradiant regime corresponds to the pronounced collective decay observed for  $r_{SR} < \lambda_I/2$ .

As shown in Fig. 1c, the signal photons are generated under continuous excitation and exhibit Bose-Einstein statistics. When the triggering signal photon defines start

time (gray dashed lines), the heralded idler photons appear in a pulsed temporal mode, corresponding to second-order cross-correlation function of the photon pair.

As the average interatomic distance  $r_{SR}$  decreases below the wavelength  $\lambda_I$  of the idler photon, the superradiant effect manifests itself as a pronounced temporal narrowing of the biphoton wavefunction, as illustrated in Fig. 1d. This sharp temporal feature of the heralded idler photon constitutes clear evidence of superradiance in the HSSR process realized in the dense thin vapor cell.

*Superradiant decay rate.*—Considering the superradiant decay rate of the idler-photon mode, the temporal wavefunction of HSSR for an atomic velocity  $v$  can be written as  $\Psi_v(\tau) \equiv \langle 0 | \hat{a}_I(t_I) \hat{a}_S(t_S) | \Psi_v \rangle$ , where  $\hat{a}_S(t_S)$  and  $\hat{a}_I(t_I)$  denote the annihilation operators for the signal and idler photons measured at times  $t_S$  and  $t_I$ , respectively, and  $\tau = t_I - t_S$  is the detection-time difference.

The  $\Psi_v(\tau)$  can be described as follows,

$$\Psi_v(\tau) = A(v) e^{(-\Gamma_{SR}/2 + ik_I v)\tau}, \quad (2)$$

where  $k_I$  is the idler-photon wavevector, and  $A(v)$  is a velocity-dependent complex amplitude that quantifies the degree of two-photon coherence generated in each velocity group. (Methods) The superradiant decay rate  $\Gamma_{SR}$  of the idler mode is described by

$$\Gamma_{SR} = \Gamma_I (1 + \mu N), \quad (3)$$

where,  $\Gamma_I$  is the intrinsic decay rate of the idler photon mode of the  $6S_{1/2}$ – $6P_{3/2}$  transition and  $\mu$  denotes geometrical constant<sup>22</sup>, assuming emitters distributed within a cylindrical volume (Methods).

The superradiant enhancement depends critically on the average interatomic distance  $r_{SR}$ , which is governed by the temperature of the atomic vapor cell. The number of atoms  $N$  within the interaction volume, and the corresponding  $r_{SR}$  are calculated from the temperature-dependent vapor pressure of cesium atoms and the cylindrical interaction volume<sup>23</sup>. Using the known relation between vapor pressure and atomic number density,  $N$  and  $r_{SR}$  can be written as

$$r_{SR} = \frac{5}{9} \left( \frac{N}{V} \right)^{-\frac{1}{3}}, \quad (4)$$

where  $V$  is the interaction volume. Substituting Equation(4) into Equation(3) yields the superradiant decay rate as follows:

$$\Gamma_{SR} = \Gamma_I \left[ 1 + \mu \frac{V}{\lambda_I^3} \left( \frac{9}{5} \frac{r_{SR}}{\lambda_I} \right)^{-3} \right]. \quad (5)$$

The second-order cross-correlation function  $g_{\text{SI}}^{(2)}(\tau)$  for the HSSR generated from a Doppler-broadened atomic ensemble is defined as<sup>24,25</sup>

$$g_{\text{SI}}^{(2)}(\tau) = \left| \int \Psi_v(\tau) f(v) dv \right|^2 H(\tau), \quad (6)$$

where  $f(v)$  is a one-dimensional Maxwell-Boltzmann velocity distribution function, and  $H(\tau)$  is the Heaviside step function. The temporal shape of Equation(6) corresponds to the temporal two-photon wavefunction, related to the temporal behaviour of the cascade-type HSSR process. We can describe  $g_{\text{SI}}^{(2)}(\tau)$ , integrated with the velocity  $v$  of atoms with a one-dimensional Maxwell-Boltzmann velocity distribution along the propagation direction of the pump beam (Methods). Here, because  $\Psi_v(\tau)$  of Equation(2) is included the  $\Gamma_{\text{SR}}$  superradiant decay rate of the idler photon mode, the temporal width of  $g_{\text{SI}}^{(2)}(\tau)$  becomes narrower as  $\Gamma_{\text{SR}}$  increases.

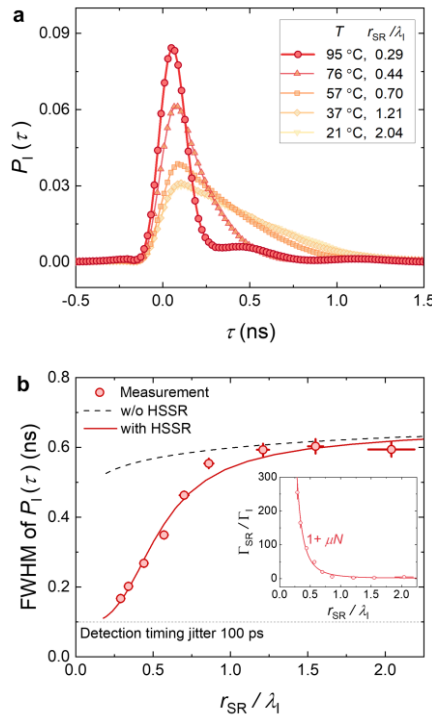


**Fig. 2 Superradiance of heralded idler photon.** **a**, Normalized temporal probability distribution  $P_I(\tau)$  of the heralded idler photons measured at different vapor cell temperatures. Increasing temperature leads to clear superradiant temporal narrowing. **b**, Temporal width (FWHM) of the heralded idler photon as a function of the ratio  $r_{\text{SR}}/\lambda_I$ . The data agree with the superradiant (red curve), whereas the Doppler-only model (black dashed curve) does not reproduce the observed narrowing. The gray dotted line indicates the 100 ps detection-timing jitter. The inset shows extracted superradiance strength. (Methods)

*Superradiance of heralded idler photon.*—To confirm the superradiance of the heralded idler photons arising from cascade-type HSSR, we investigate how the temporal waveform of the heralded idler photons depends on the average interatomic distance  $r_{\text{SR}}$ . In our experiment,  $r_{\text{SR}}$  is controlled by varying the temperature of the cesium vapor cell, which determines the atomic number density. From Equation(4), we estimate  $r_{\text{SR}}$  as a function of temperature: as the cell temperature increases from 21 °C to 95 °C,  $r_{\text{SR}}$  decreases from  $2\lambda_I$  to 0.29  $\lambda_I$ . To quantify the superradiance, we define the normalized temporal probability distribution of the heralded idler photon as

$$P_I(\tau) = \frac{g_{\text{SI}}^{(2)}(\tau)}{\int d\tau g_{\text{SI}}^{(2)}(\tau)}, \quad (7)$$

which gives the temporal probability of detecting a heralded idler photon per detected signal photon.

We measured  $P_I(\tau)$  while varying the Cs vapor-cell temperature from the 21 °C to 95 °C, as shown in Fig. 2a. At a cell temperature of 57 °C, corresponding to  $r_{\text{SR}} \approx 0.7\lambda_I$ , a pronounced sharp temporal feature appears in the heralded-idler waveform. In this subwavelength regime ( $r_{\text{SR}} < \lambda_I$ ), the temporal peak becomes significantly narrower, indicating the onset of a superradiance triggered by the signal photon.

We further analyse the temporal width of  $P_I(\tau)$  as a function of the ratio of  $r_{\text{SR}}/\lambda_I$ , as summarized in Fig. 2b. The inset in Fig. 2b shows the superradiance strength  $\Gamma_{\text{SR}}/\Gamma_I$ , extracted by comparing the measured temporal widths with the theoretical linewidth obtained from Equation(6) after convolution with detection timing jitter (Methods). As the cell temperature increases and  $r_{\text{SR}}$  decreases, the temporal width of  $P_I(\tau)$  narrows significantly from 0.60 ns to 0.17 ns. Even in the regime where  $r_{\text{SR}} < \lambda_I$ , a clear compression of the temporal width of  $P_I(\tau)$  is observed, which becomes more pronounced as  $r_{\text{SR}}$  approaches and drops below  $\lambda_I$ .

The measured temporal widths agree well with the theoretical curve (red solid line in Fig. 2b), calculated from Equation(7), which incorporates the superradiant decay rate  $\Gamma_{\text{SR}}$  of Equation(3) and is convolved with the detection timing jitter (Methods). We also compare the data with the linewidth expected solely from the thermal velocity distribution of atoms (black dashed line). Notably, once the system enters the subwavelength regime, the observed reduction in the FWHM of  $P_I(\tau)$  is far stronger than the Doppler-induced narrowing predicted by this model.

In contrast, the Doppler-only model fails to reproduce the measured compression, whereas the experimental trend shows a much more rapid narrowing with temperature. This

strong temperature-dependent reduction of the  $P_1(\tau)$  width provides clear evidence of a superradiance in our cascade-type four-wave mixing system.

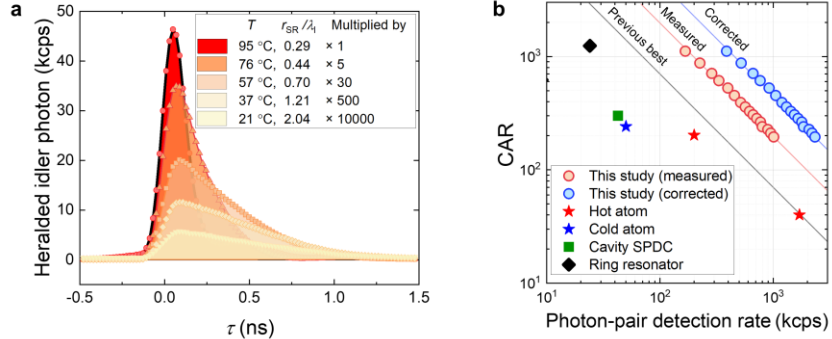


**Fig. 3 Brightness enhancement via heralded single-photon superradiance.** **a**, Heralded idler photon counts measured at different cesium vapor cell temperatures. Each curve corresponds to a distinct temperature, with the associated average interatomic distance  $r_{SR} / \lambda_1$  indicated in the legend. For clarity of presentation, the lower temperature traces are multiplied by  $\times 5$ ,  $\times 30$ ,  $\times 500$ , and  $\times 10000$ . **b**, Photon-pair detection rate versus CAR, including results from different photon-pair generation platforms. The red circles represent measured results and the blue circles indicate the expected performance assuming improved detector quantum efficiency.

*Efficiency of superradiance in atomic system.*—Owing to superradiance in the cascade-type HSSR process, our dense 1-mm-long cesium vapor cell yields a highly bright photon-pair source. Fig. 3a shows the heralded idler-photon counts measured over 30 s while varying the cell temperature, with a fixed pump power of 0.06 mW and a coupling power of 15 mW. Each histogram bin corresponds to 5 ps. At a cell temperature of 95 °C, our HSSR source exhibits a coincidence-to-accidental ratio (CAR) of 200 and a detected photon-pair rate exceeding  $10^6$  pairs/s. As the temperature increases, the number of participating atoms per unit volume and the superradiance rises, leading to higher brightness through enhanced pair generation over four-order ( $10^4$ ) comparing with the case of  $r_{SR} \geq \lambda_1$ . At the same time, stronger superradiant coupling shortens the temporal width of the correlation function, indicating faster collective emission dynamics and resulting in an increased CAR.

A further advantage of the thin vapor cell is that bright emission can be sustained even under high optical depth (OD) conditions. Across reported results, the optimal OD for maximizing heralding efficiency increases as the cell length decreases: approximately 4 for 25 mm<sup>26</sup>, 12 for 5 mm<sup>27</sup>, and 20 for a 1 mm cell used here. This trend is attributed to reduced reabsorption. Under strong superradiant emission, the idler spectrum broadens beyond the atomic absorption linewidth, which suppresses reabsorption and enables bright photon-pair generation at higher OD.

Fig. 3b compares our photon-pair source with previously reported narrow-bandwidth (linewidths below a few gigahertz) photon-pair systems, which are advantageous for quantum memory and fiber-based communication<sup>14,28</sup>. The plot shows the photon-pair detection rate, rather than generation rate, versus CAR to provide a practical comparison based on directly measurable quantities that inherently include optical losses. The blue circles represent data obtained with a 15 mW coupling laser while varying the pump power from 0.01 to 0.16 mW, and the red circles indicate the expected performance assuming improved detector quantum efficiency. Other symbols correspond to reported results from four-wave mixing in micro-ring resonators<sup>29</sup>, SPDC in optical cavities<sup>30</sup>, cold-atom ensembles<sup>31</sup>, and warm atomic vapors<sup>26,27</sup>. The solid lines trace the reported relationships between CAR and photon-pair detection rate derived from the best-performing results. For OD=20 and a pump power of 0.16 mW, the heralding efficiency is 22% without correcting for the detector quantum efficiency and increases to 37% after correction. Under the same condition, a CAR of 200 corresponds to a photon-pair detection rate of  $10^6$  pairs/s, which increases to  $2.85 \times 10^6$  pairs/s after accounting for the detector efficiency. These results demonstrate that our HSSR-based source outperforms previous implementations in both brightness and correlation, highlighting the capability of superradiant emission in a thin vapor cell to generate bright, highly correlated photon-pair source.

**Summary.**—We have demonstrated bright heralded single-photon superradiance in a thin dense  $^{133}\text{Cs}$  vapor cell via spontaneous four-wave mixing. Using a 1-mm thin vapor cell at high atomic density, we reduce the average interatomic distance into the subwavelength regime, where photon pairs exhibit temporal narrowing to 0.17 ns, far beyond what can be explained by Doppler effects. This behavior provides clear evidence of cooperative superradiant emission. Thermal vapor cells offer an exceptionally convenient means of tuning optical depth through temperature, which allows continuous access to both dilute and subwavelength regimes. This tunability directly controls the strength of superradiance and makes thermal vapors a versatile platform for studying superradiance. In the subwavelength regime, our photon-pair source achieves a CAR of 200 and a photon-pair detection rate of  $10^6$  (expected rate  $>10^7$ ) pairs per second, demonstrating the brightest photon-pair source realized in a thermal atomic system to date and highlighting the practical utility of superradiance in quantum photonic applications. These results mark a significant step toward high brightness, correlated quantum light sources in thermal media. To our knowledge, this constitutes the brightest photon pair source reported to date, establishing hot atomic vapors as a practical and scalable platform for superradiant nonlinear optics. By tuning the superradiance strength, the temporal width and spectral properties of the photon-pair can be actively controlled, demonstrating that cooperative emission in warm atomic ensembles provides a scalable and versatile platform that can be readily integrated into hybrid quantum systems for quantum communication and quantum networking.

## References

- 1 Dicke, R. H. Coherence in spontaneous radiation processes. *Phys. Rev.* **93**, 99 (1954).
- 2 Jahnke, F. *et al.* Giant photon bunching, superradiant pulse emission and excitation trapping in quantum-dot nanolasers. *Nat. Commun.* **7**, 11540 (2016).
- 3 Angerer, A. *et al.* Superradiant emission from colour centres in diamond. *Nat. Phys.* **14**, 1168-1172 (2018).
- 4 Masson, S. J., Covey, J. P., Will, S. & Asenjo-Garcia, A. Dicke superradiance in ordered arrays of multilevel atoms. *PRX Quantum* **5**, 010344 (2024).
- 5 Seo, B. *et al.* Mirror symmetry breaking of superradiance in a dipolar Bose-Einstein condensate. *Phys. Rev. Res.* **6**, L042028 (2024).
- 6 Ferioli, G., Ferrier-Barbut, I. & Browaeys, A. Emergence of second-order coherence in the superradiant emission from a free-space atomic ensemble. *Phys. Rev. Lett.* **134**, 153602 (2025).
- 7 Eberly, J. H. Emission of one photon in an electric dipole transition of one among N atoms. *J. Phys. B-At. Mol. Opt. Phys.* **39**, S599 (2006).
- 8 Scully, M. O., Fry, E. S., Ooi, C. R. & Wódkiewicz, K. Directed spontaneous emission from an extended ensemble of N atoms: timing is everything. *Phys. Rev. Lett.* **96**, 010501 (2006).
- 9 Jen, H.-H. Superradiant cascade emissions in an atomic ensemble via four-wave mixing. *Ann. Phys.* **360**, 556-570 (2015).
- 10 Lee, Y.-S., Lee, S. M., Kim, H. & Moon, H. S. Single-photon superradiant beating from a Doppler-broadened ladder-type atomic ensemble. *Phys. Rev. A* **96**, 063832 (2017).
- 11 Whiting, D. J., Šibalić, N., Keaveney, J., Adams, C. S. & Hughes, I. G. Single-photon interference due to motion in an atomic collective excitation. *Phys. Rev. Lett.* **118**, 253601 (2017).
- 12 Kim, H., Jeong, H. & Moon, H. S. Collective biphoton temporal waveform of photon-pair generated from Doppler-broadened atomic ensemble. *Quantum Sci. Technol.* **9**, 045006 (2024).
- 13 Duan, L.-M., Lukin, M. D., Cirac, J. I. & Zoller, P. Long-distance quantum communication with atomic ensembles and linear optics. *Nature* **414**, 413-418 (2001).
- 14 Lvovsky, A. I., Sanders, B. C. & Tittel, W. Optical quantum memory. *Nat. Photonics* **3**, 706-714 (2009).
- 15 Hosseini, M., Sparkes, B. M., Campbell, G., Lam, P. K. & Buchler, B. C. High efficiency coherent optical memory with warm rubidium vapour. *Nat. Commun.* **2**, 174 (2011).
- 16 Park, J., Kim, H. & Moon, H. S. Polarization-entangled photons from a warm atomic ensemble using a Sagnac interferometer. *Phys. Rev. Lett.* **122**, 143601 (2019).
- 17 Craddock, A. N. *et al.* Automated distribution of polarization-entangled photons using deployed New York City fibers. *PRX Quantum* **5**, 030330 (2024).
- 18 Park, J., Jeong, T., Kim, H. & Moon, H. S. Time-Energy Entangled Photon Pairs from Doppler-Broadened Atomic Ensemble via Collective Two-Photon Coherence. *Phys. Rev. Lett.* **121**, 263601 (2018).
- 19 Park, J., Kim, H. & Moon, H. S. Four-Photon Greenberger-Horne-Zeilinger Entanglement via Collective Two-Photon Coherence in Doppler-Broadened Atoms. *Adv. Quantum Technol.* **4**, 2000152 (2021).
- 20 Jeong, T., Lee, Y.-S., Park, J., Kim, H. & Moon, H. S. Quantum interference between autonomous single-photon sources from Doppler-broadened atomic ensembles. *Optica* **4**, 1167-1170 (2017).
- 21 Park, J., Kim, H. & Seb Moon, H. Entanglement swapping with autonomous polarization-entangled photon pairs from a warm atomic ensemble. *Opt. Lett.* **45**, 2403-2406 (2020).
- 22 Rehler, N. E. & Eberly, J. H. Superradiance. *Phys. Rev. A* **3**, 1735 (1971).
- 23 Alcock, C. B., Itkin, V. & Horrigan, M. Vapour pressure equations for the metallic elements: 298–2500K. *Can. Metall. Q.* **23**, 309-313 (1984).
- 24 Ding, D.-S., Zhou, Z.-Y., Shi, B.-S., Zou, X.-B. & Guo, G.-C. Generation of non-classical correlated photon pairs via a ladder-type atomic configuration: theory and experiment. *Opt. Express* **20**, 11433-11444 (2012).
- 25 Du, S., Wen, J. & Rubin, M. H. Narrowband biphoton generation near atomic resonance. *J. Opt. Soc. Am. B* **25**, C98-C108 (2008).
- 26 Davidson, O., Yoge, O., Poem, E. & Firstenberg, O. Bright, low-noise source of single photons at 780 nm with improved phase-matching in rubidium vapor. *arXiv preprint arXiv:2301.06049* (2023).
- 27 Craddock, A. N. *et al.* High-rate subgigahertz-linewidth bichromatic entanglement source for quantum networking. *Phys. Rev. Appl.* **21**, 034012 (2024).
- 28 Sena, M. *et al.* High-fidelity quantum entanglement distribution in metropolitan fiber networks with co-propagating classical traffic. *J. Opt. Commun. Netw.* **17**, 1072-1081 (2025).
- 29 Fan, Y. R. *et al.* Multi-wavelength quantum light sources on silicon nitride micro-ring chip. *Laser Photon. Rev.* **17**, 2300172 (2023).
- 30 Li, Y.-H. *et al.* Compact sub-GHz bandwidth single-mode time-energy entangled photon source for high-speed quantum networks. *OSA Continuum* **4**, 608-620 (2021).
- 31 Shiu, J.-S. *et al.* Observation of highly correlated ultrabright biphotons through increased atomic ensemble density in spontaneous four-wave mixing. *Phys. Rev. Res.* **6**, L032001 (2024).

## Methods

### Experimental setup

The experiment was performed using a 1-mm-long cesium vapor cell. The pump and coupling beams were counter-propagating and overlapped in the center of the cell with a beam waist of  $78 \mu\text{m}$  ( $1/e^2$  radius). A continuous-wave pump laser at 852 nm was blue-detuned from the  $6S_{1/2}(F=4) \rightarrow 6P_{3/2}(F'=5)$  transition by  $\delta_p = 1.31\text{GHz}$ . The coupling laser at 917 nm was red-detuned from the  $6P_{3/2}(F'=5) \rightarrow 6D_{5/2}(F''=6)$  transition by  $\delta_c = -1.35\text{GHz}$ . The resulting two-photon detuning was  $\delta_{\text{two}} = \delta_p + \delta_c = -0.04\text{GHz}$ . The pump power was varied between 0.01 mW and 0.16 mW, whereas the coupling power was kept constant at 15 mW. The generated signal and idler photons pass through a band pass filter and polarizer to remove residual laser components, after which they are coupled into a single-mode fiber and delivered to the detectors. For photon detection, we employ superconducting nanowire single-photon detectors (SNSPDs) optimized for 780 nm. The quantum efficiencies of detectors are 70 % for 852 nm, and 50% for 917 nm, respectively, and the timing jitter of the detector is approximately 70 ps (FWHM).

#### Optical depth and average interatomic distance

To determine the optical depth (OD), we used a weak 852 nm probe beam resonant with the  $6S_{1/2}(F=4) \rightarrow 6P_{3/2}(F'=5)$  transition. A probe beam power of  $0.1 \mu\text{W}$  ensured operation within the linear, unsaturated absorption regime. The OD was extracted by comparing the probe intensity before and after transmission through the vapor cell, using the relation

$$I_{\text{out}} = I_{\text{in}} e^{-\text{OD}}$$

Using the temperatures obtained from the OD measurements, together with the known temperature-pressure relation of  $^{133}\text{Cs}$ , the average interatomic distance can be calculated by applying Equation(4). For each experimental condition, the measured OD and the corresponding cell temperature and average interatomic distance are summarized in Extended Data Table 1.

#### Second-order cross-correlation function $g_{\text{SI}}^{(2)}(\tau)$ for HSSR

For cascade-type warm atomic ensembles, the second-order correlation function is reported<sup>24,25</sup>. By incorporating the increased decay rate due to superradiance in the idler photon, the function becomes:

$$g_{\text{SI}}^{(2)}(\tau) = \left| \int_{-\nu}^{\nu} dv \frac{1}{\sqrt{\pi u}} e^{-\frac{v^2}{u}} \frac{C}{[(2\Gamma_I + 4i(\delta_p - k_p v)) \{ \Gamma_S + i(-k_p + k_c) v \} + \Omega_c^2]} e^{ik_p v \tau} e^{\frac{\Gamma_{\text{SR}}}{2} \tau^2} \right| H(\tau),$$

Here,  $v$  denotes the atomic velocity,  $u$  is the most probable speed,  $\Gamma$  represents the decay rate,  $\delta$  is the detuning,  $k$  is the wave number corresponding to the optical momentum, and  $\tau$  is the time difference between the signal and idler detections.  $H(\tau)$  denotes the Heaviside function, and the subscripts P, C, S, and I correspond to the pump, coupling, signal, and idler fields or their respective energy levels.  $C$  is a proportionality constant that scales with the number of atoms and the transition probability, characterizing the overall interaction strength, and  $\Gamma_{\text{SR}}$  is defined as  $\Gamma_{\text{SR}} = \Gamma_I(1 + \mu N)$ .

By defining  $A(v)$  as follows, the expressions in Equation(2) can be written in a more compact form.

$$A(v) = \frac{C}{[(2\Gamma_I + 4i(\delta_p - k_p v)) \{ \Gamma_S + i(-k_p + k_c) v \} + \Omega_c^2]}$$

In the experiment, the temporal response was influenced by the jitter of the detectors and the time-correlated single-photon counting (TCSPC) system, which was modeled as a Gaussian jitter with a full width at half maximum (FWHM) of approximately 100 ps. In Fig. 2b, the theoretical curves were convolved with this jitter profile to compare with the measured data.

#### Superradiance strength

Because the atoms are randomly distributed within the medium, a correction term accounting for the spatial distribution is required. To quantify the superradiant effect, we evaluated the superradiance strength  $\Gamma_{\text{SR}}/\Gamma_I$  by comparing the measured  $g_{\text{SI}}^{(2)}(\tau)$  width with the theoretical model.

Fig. 2 inset shows the superradiance strength as a function of the average interatomic distance at different temperatures. The experimental results were fitted using the relation  $\Gamma_{\text{SR}}/\Gamma_I = 1 + \mu N$  where  $\mu$  is a geometric constant describing the emitters distributed within a cylindrical volume.

The experimental data show excellent agreement with the model, yielding  $\mu = (1.15 \pm 0.08) \times 10^{-6}$ . This value of  $\mu$  was subsequently used to calculate the theoretical curves presented in Fig. 1d, Fig 2b, and Extended Data Fig. 2.

#### Temperature-dependent simulation superradiant emission

Based on the experimentally determined decay rate and Equation(4), the intensity of the idler photons as a function of temperature, as well as the probability distribution for detecting an idler photon after a signal photon, can be simulated. An increase in the temperature of the warm atomic ensemble not only reduces the average interatomic distance but also increases the total number of atoms in the vapor cell. Consequently, as shown in Extended Data Fig. 1a, the overall brightness is expected to increase with temperature, which is in good agreement with the measurements obtained over 30 s for each temperature.

When the results in Extended Data Fig. 1b are normalized by their total area to compare the probability distributions, the results in Extended Data Fig. 1a are obtained. As the cell temperature rises from room temperature, little change is observed while the mean interatomic distance remains larger than the idler wavelength. However, as the interatomic distance becomes smaller than the idler wavelength, the decay rate is further enhanced by superradiance, causing the width of the probability distribution to become narrower. This behavior is consistent with the tendency observed in Fig. 2a and Fig. 3a.

#### Acknowledgements

This work was supported by Institute for Information and Communications Technology Promotion (RS-2024-00396999, IITP-2025-RS-2020-II201606, RS-2022-

II221029, RS-2025-25464481); National Research Foundation of Korea (RS-2023-00283146, RS-2025-25454381).

#### **Competing interests**

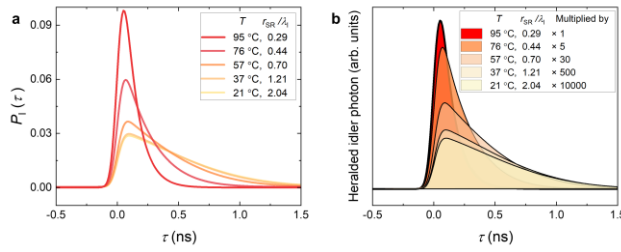
The authors declare no competing interests.

---

**Cell temperature (°C)      OD       $r_{SR}/\lambda_I$** 

21	0.06(1)	2.04(15)
29	0.14(1)	1.55(5)
37	0.29(2)	1.21(4)
49	0.76(6)	0.86(3)
57	1.5(1)	0.70(3)
65	2.7(2)	0.57(2)
76	5.6(4)	0.44(1)
87	12(1)	0.34(1)
95	20(2)	0.29(1)

**Extended Data Table 1** Measured optical depth and corresponding cell temperature and interatomic distance ratio  $r_{SR}/\lambda_I$ . The OD is obtained from the transmission on the transition  $6S_{1/2}(F=4) \rightarrow 6P_{3/2}(F'=5)$  transition.



**Extended Data Fig. 1** Simulated temperature dependence of the raw and normalized idler photon count. **a**, Brightness of the idler photons as a function of cell temperature. The inset shows the cell temperatures and the corresponding interatomic distance ratio relative to the idler wavelength. Multiplying factors are applied for clarity in comparing the magnitudes. **b**, Normalized cross-correlation functions illustrating the narrowing effect with increasing temperature.